Korean J. Chem. Eng., 40(12), 2800-2814 (2023)
DOI: 10.1007/s11814-023-1540-x

pISSN: 0256-1115
eISSN: 1975-7220

Analysis of the total energy consumption through hydrogen compression for the operating pressure optimization of an alkaline water electrolysis system

Yongbeom Shin, Jongyeon Oh, and Dongil Shin†

Department of Chemical Engineering, Myongji University, 116 Myongji-ro, Cheoin-gu, Yongin, Gyeonggido 17058, Korea
(*Received 10 April 2023 • Revised 7 July 2023 • Accepted 25 July 2023*)

Abstract−Green hydrogen, produced through the water electrolysis system, needs to be compressed to 200-700 bar for transportation, storage, and charging. Thus, it is necessary to consider the compression process of the produced hydrogen. In this study, an alkaline water electrolysis cell model was developed, and a system simulation model was proposed by integrating it into gPROMS. Total energy consumption and efficiency, according to operational conditions, were analyzed by considering the energy consumption for hydrogen compression to 200 bar through the developed model. The optimal operating pressure demonstrated in the previous study was less than 10 bar when the compression process was not considered. However, the energy efficiency was highest at 10-30 bar with the energy required for hydrogen compression. Nonetheless, a high-pressure operation may be subject to material restrictions or legal regulations. Therefore, material constraints and social regulations should be simultaneously considered to minimize the operating costs and maximize energy efficiency.

Keywords: Alkaline Water Electrolysis System, Green Hydrogen, Hydrogen Production and Compression, Total Energy Consumption, Hydrogen Production Efficiency

INTRODUCTION

The world is experiencing climate extremes such as heatwaves, heavy snowfalls, and typhoons due to global warming, and the international community has adopted the Paris Agreement, which aims to keep the global average temperature rise within 1.5 °C. In 2018, the scientific basis for the 1.5 °C target was prepared in the "Global Warming 1.5 °C Special Report" approved at the Intergovernmental Panel on Climate Change (IPCC) General Assembly to limit the global average temperature rise to 1.5 °C, the necessity of reducing carbon dioxide emissions by 45% by 2030 and realizing carbon neutrality by 2050 was suggested [1]. To achieve the goal, Sweden, the United Kingdom, France, Denmark, New Zealand, and Hungary have enacted carbon neutrality, and countries such as China, Japan, and Korea have declared the 2050 carbon neutrality. It can contribute to achieving carbon neutrality by reducing carbon emissions in the atmosphere by converting major energy sources, from fossil fuels to renewable energy, and R&D investment is required to expand the proportion of renewable energy generation [2]. As of 2020, the share of renewable energy in electricity generation in the European Union surpassed fossil fuels, and in the case of the United States, it became the second-highest energy source, and consequently, the share of renewable energy generation is steadily increasing [3,4].

When the amount of renewable energy generation increases, it is necessary to adjust the supply amount according to demand to maintain the stability of the power grid [5]. However, it is necessary to store and supply energy according to the demand due to the characteristic of renewable energy, which is highly volatile and the amount of power generation cannot be controlled; thus it is required to expand about five times to 120 GW in the United States by 2050 [6]. Representative surplus energy storage methods include pumped storage hydropower, thermal energy storage, flywheel, and power-to-gas (P2G); pumped storage hydropower is unprofitable in countries with small land areas, and thermal energy storage and flywheel are not suitable for long-term storage of large-capacity electricity [7]. P2G, which stores energy through hydrogen produced by electrolysis of water with surplus energy, is less affected by the season and can be transported to various energy demand areas since it uses hydrogen as a medium for energy storage and transportation, which is an eco-friendly energy source that does not emit carbon [8].

However, it is necessary to secure price competitiveness to expand the supply of green hydrogen produced from surplus energy. According to the International Renewable Energy Agency [9], gray hydrogen, which accounts for the largest portion of the current hydrogen production method, is produced through natural gas or methane reforming. Blue hydrogen reduces carbon emissions by capturing and storing carbon generated in the production process to overcome the disadvantages of gray hydrogen. On the other hand, the production cost of green hydrogen, an eco-friendly energy source, is $3-7.2 per kg, which is up to five times higher than that of gray hydrogen. In order to secure the price competitiveness of green hydrogen, the International Renewable Energy Agency has proposed three major methods as follows: 1) The first method is a scale-up of the water electrolysis system, and the size of the water electrolysis module greatly affects the production cost. Therefore, when the 1 MW water electrolysis system is increased to 20 MW,

†To whom correspondence should be addressed.
E-mail: dongil@mju.ac.kr

the production cost is greatly reduced by more than a third. 2) The second method is to improve efficiency through the development of materials for water electrolysis systems such as electrodes or separators. 3) The third method is the efficient operation of the water electrolysis system. As the operation time of the water electrolysis system increases, the cost of electricity is dominant rather than the equipment and operation cost of the water electrolysis system [9].

Alkaline water electrolysis (AWE), polymer electrolyte membrane water electrolysis (PEM), and solid oxide water electrolysis cell (SOEC) are representative of water electrolysis systems. Among them, the AWE system, which has the highest technological maturity and the advantage of the low equipment cost because expensive electrochemical catalysts are not used, is widely used [10,11]. The AWE system-linked renewable energy is operated at various current densities due to large load fluctuations, causing a decrease in system efficiency [12]. In addition, since the hydrogen produced in the AWE system is compressed to high pressure of 200 bar or more for storage, the operation of the AWE system at high pressure is considered to improve the overall system efficiency [13]. Studies are required to derive the optimal operating conditions for the AWE system linked with renewable energy considering a wide range of current density, temperature, and operating pressure.

Ullerberg [14] developed a mathematical model of an AWE system based on theories of thermodynamics, heat transfer, and electrochemistry. The developed model predicts the dynamic characteristics of cell voltage, hydrogen production, system efficiency, and temperature, and the prediction performance was verified by comparing with the actual measurement data of the solar-powered hydrogen production plant in Julich, Germany. By integrating the AWE system model with the fuel cell and hydrogen storage model, a simulation of a solar-linked hydrogen production plant was performed, and the operation strategy of the water electrolysis system, the amount of fuel cell usage, and the hydrogen storage pressure were proposed. Hammoudi et al. [15] developed a mathematical model using the structural characteristics of the water electrolysis system as parameters to overcome the disadvantage of having to collect several weeks of experimental data to estimate the parameters of the previous AWE model. The developed model can simulate energy consumption, efficiency, and hydrogen production in Matlab's Simulink; the energy consumption of the AWE system was analyzed in the pressure range of 1-70 bar. Henao et al. [16] developed an AWE system model that reflects the characteristics of materials used in electrodes, separators, and electrolytes. The developed model predicts the energy consumption of an AWE system according to temperature, pressure, and load fluctuations, and it was verified by the AWE system at the Hydrogen Research Institute (HRI) in Quebec, Canada. Abdin et al. [17] developed a generalized AWE system model, not a model for a specific system, by reflecting the physical and material properties of the AWE system as model parameters. Kojima et al. [18] conducted a simulation of the performance of an alkaline water electrolysis system according to load fluctuations using the temperature dynamic characteristics, and the performance of the water electrolysis system according to the 150 kW, 1 MW, and 5 MW scales was compared. Sanchez et al. [19] developed an entire process simulation model including the process equipment such as the AWE stack, pump, heat exchanger, separator, and condenser of an AWE system using Aspen Plus®. Using the developed model, the efficiency of the AWE system was analyzed at various temperatures (50-80 °C) and pressure (5-10 bar), and Jang et al. [20] similarly developed an Aspen simulation model of an AWE system, analyzed energy consumption and efficiency according to temperature, and tried to suggest optimal operating conditions for an alkaline water electrolysis system.

However, the hydrogen produced from the water electrolysis system is compressed at a high pressure of 200-500 bar to the cylinder of a trailer truck or 700 bar to the tank for transportation, storage, and charging. Therefore, not only water electrolysis system optimization to improve hydrogen production efficiency but also hydrogen compression should be considered [21]. To reduce the energy consumed for hydrogen compression, a water electrolysis system operated at high pressure was proposed, and the performance of the water electrolysis system according to the pressure was analyzed. Onda et al. [22] analyzed the energy consumption according to the operating pressure of the PEM electrolysis up to high pressure of 70 MPa and showed that the high-pressure water electrolysis system reduced energy consumption by 5% compared to the atmospheric pressure water electrolysis system. On the other hand, Roy et al. [23] analyzed the energy efficiency of the AWE system at pressures up to 700 atm and showed contradictory results in that the high-pressure water electrolysis system consumes 16% more energy than the atmospheric pressure water electrolysis system. Jang et al. [24] developed a model focused on the bubble effect of the AWE system in Aspen Plus®, and analyzed the energy consumption, hydrogen production, and purity for a pressure range of 1-100 bar; as a result, the optimal system efficiency was demonstrated at an operating pressure of 5-10 bar. In addition, facilities that integrate a water electrolysis system linked with renewable energy and a hydrogen refueling station are being proposed due to the difficulty of mass transportation of hydrogen. Minutillo et al. [25] performed a techno-economic analysis of a facility in which a water electrolysis system and a hydrogen refueling station were integrated, and showed that the hydrogen compression cost accounted for the second-highest proportion of about 17.4% of the total cost after the hydrogen production cost.

Hydrogen produced from water electrolysis goes through a compression process for transportation, storage, and charging; thus, hydrogen compression must be considered for system optimization, and the compressor occupies a high proportion of the energy consumption of the entire plant [26]. Previous studies suggested a high-pressure operation to reduce the energy consumed in compression, and mainly analyzed the performance change of the water electrolysis system according to the pressure change, but did not consider the energy consumption of the compressor, which consumes a high proportion of energy. The purpose of this study is to analyze the overall energy efficiency of a P2G plant including a water electrolysis system and a compressor according to operating conditions such as operating temperature, pressure, and current density. In particular, based on the fact that the produced hydrogen is compressed to a pressure of 200 bar for transport through a trailer truck, the energy consumption of the entire plant according to operating conditions was analyzed, and optimal operating conditions

to maximize plant efficiency are proposed.

In this study, an AWE system simulation model including a compressor was developed in gPROMS. For the AWE cell, the Electrochemical Cell Reactor (ECR) library provided by gPROMS was used, and the process equipment such as separator, pump, heater, condenser, and compressor was modeled using gPROMS Process 2.1.1. The ECR library provided by gPROMS is developed based on the PEM electrolysis system, for modeling the AWE cell where the electrochemical reaction takes place inside the liquid electrolyte, the movement phenomenon inside the liquid and the resistance by bubbles must be additionally considered. An AWE cell model was proposed initially in Python, and it was integrated with the ECR model using a custom modeling template in gPROMS, and extended to the entire system model including the process equipment. Using the developed AWE system, the overall efficiency according to the operating conditions was compared for both the case where the energy consumption of the compressor was not considered and the case where it was considered.

ALKALINE WATER ELECTROLYSIS SYSTEM CONFIGURATIONS

1. AWE System Description

Fig. 1 indicates a process flow diagram of an AWE system, and a simulation model was developed based on this system. In the AWE system, an electrochemical reaction (Eq. (1)) occurs in the stack, which produces hydrogen at the cathode (Eq. (2)) and oxygen at the anode (Eq. (3)), and the reaction formula is as follows [14]:

$$H_2O(l) + \text{Electrical energy} \rightarrow H_2(g) + \frac{1}{2}O_2(g) \quad (1)$$

$$\text{Cathode: } 2H_2O + 2e^- \rightarrow H_2 + 2OH^- \quad (2)$$

$$\text{Anode: } 2OH^- \rightarrow \frac{1}{2}O_2 + H_2O + 2e^- \quad (3)$$

From the gas produced in the AWE stack, the liquid KOH electrolyte contained in the gas is separated by the gas/liquid separator, and the separated liquid is supplied to the water electrolysis stack again through a heater and a pump. At this time, since a reaction in which water is consumed occurs at the cathode, water is additionally supplied to the gas/liquid separator on the cathode side to keep the concentration of the KOH solution inside the water electrolysis stack constant. The gas separated in the gas/liquid separator is finally separated from the liquid contained in the gas through a condenser and separator to increase the purity of the gas to more than 99%. Since high-purity hydrogen produced from the water electrolysis system is transported or stored as compressed hydrogen through a compressor, a compressor was additionally considered assuming that a system loads the produced hydrogen at 200 bar to a tube trailer which is the common way to transport the produced hydrogen in Korea.

2. Hydrogen Compression

Since hydrogen has a large specific volume, high-pressure compression or liquefaction is required for transportation and storage. And a renewable energy-linked AWE system is a large-scale system that is mainly installed in coastal areas with an abundant source of renewable energy. As a result, transportation is generally required from the hydrogen production plant to the demand area, so it needs to compress at a pressure of 200-500 bar. In addition, hydrogen vehicles or buses are usually charged at a high pressure of 700 bar [24]. Therefore, the compression of hydrogen in a P2G plant should be considered essentially for the actual transporta-

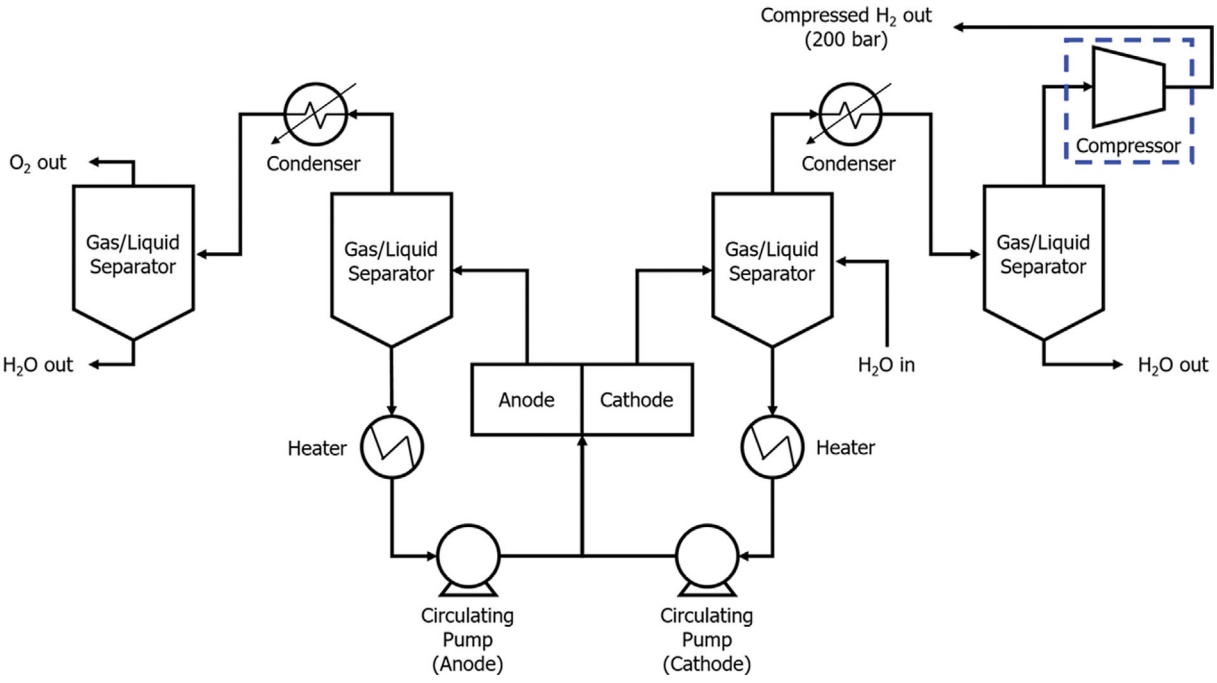

Fig. 1. Alkaline water electrolysis system configuration.

tion and utilization of green hydrogen.

In this study, it is assumed that the produced hydrogen is compressed at a pressure of 200 bar to transport it to a hydrogen refueling station in the city. The system efficiency, which was analyzed only for the hydrogen production by the AWE system, was expanded to the hydrogen compression, and the energy required to compress the hydrogen produced from the AWE system to 200 bar was considered. The optimal operating pressure of an AWE system was analyzed in various operating temperatures and current density ranges by comparing the case in which hydrogen compression was not considered and the case including hydrogen compression.

SIMULATION MODEL DEVELOPMENT

1. AWE Model Description

Fig. 2 shows the components and relationships of the developed AWE system simulation model. The AWE system simulation model consists of an AWE stack model that produces hydrogen through an electrochemical reaction and a process equipment model for separating and compressing the produced hydrogen. Since the ECR library which was used for the AWE stack simulation is a library based on the PEM electrolysis system, it is necessary to reflect the resistance and bubble effect inside the liquid electrolyte and the change in reversible voltage to model an AWE system using a liquid KOH electrolyte rather than a polymer electrolyte. The AWE cell model for cell voltage was initially developed in Python, and the AWE stack model that integrates the cell voltage model (in Fig. 2) with the ECR library through a custom modeling template in gPROMS was proposed. For the process of separation and compression of the produced hydrogen, process equipment models such as separator, pump, heater, condenser, and compressor provided by gPROMS were used. The AWE system simulation model was developed by integrating the AWE stack and process equipment in the gPROMS Process 2.1.1.

2. AWE Cell Model in Python

In the AWE cell, water is decomposed by electrical energy to produce hydrogen and oxygen; an electrochemical reaction that has positive Gibbs energy (ΔG^o=237 kJ/mol) at standard conditions is a non-spontaneous reaction. Since the electric energy required for the reaction is a crucial variable in the AWE cell in which a non-spontaneous reaction takes place, the reversible voltage which is the theoretical minimum electrical energy required for hydrogen production must be explained, and it can be expressed using Gibbs energy as follows [14]:

$$V_{rev}=\frac{\Delta G}{zF} \tag{4}$$

where z is the number of electrons exchanged per reaction (z=2), F is the Faraday constant, and G is the Gibbs energy. The reversible voltage, a thermodynamic model expressed through Gibbs energy, can be expressed in terms of temperature and pressure using the Nernst equation, and is as follows [24]:

$$V_{rev}=V_{rev}^{o}+\frac{RT}{2F}\ln\left(\frac{(P-P_{H_2O})^{1.5}P_{H_2O}^{*}}{P_{H_2O}}\right) \tag{5}$$

where P, T, R, F are pressure (bar), temperature (K), gas constant, and Faraday constant, P_{H_2O} is the vapor pressure of the electrolyte (bar), and $P_{H_2O}^{*}$ is the vapor pressure of pure water (bar). The vapor pressure of the electrolyte P_{H_2O} and the vapor pressure of pure water $P_{H_2O}^{*}$, which are variables of the reversible potential model using the Nernst equation, can be calculated as follows [27]:

$$P_{H_2O}=T^{-3.498}\exp\left(37.93-\frac{6426.32}{T}\right)\times(0.016214-0.13082m+0.1933m^{0.5}) \tag{6}$$

$$m=w\frac{183.1221-0.56845T+984.5679\exp\left(\frac{w}{115.96277}\right)}{5610.5} \tag{7}$$

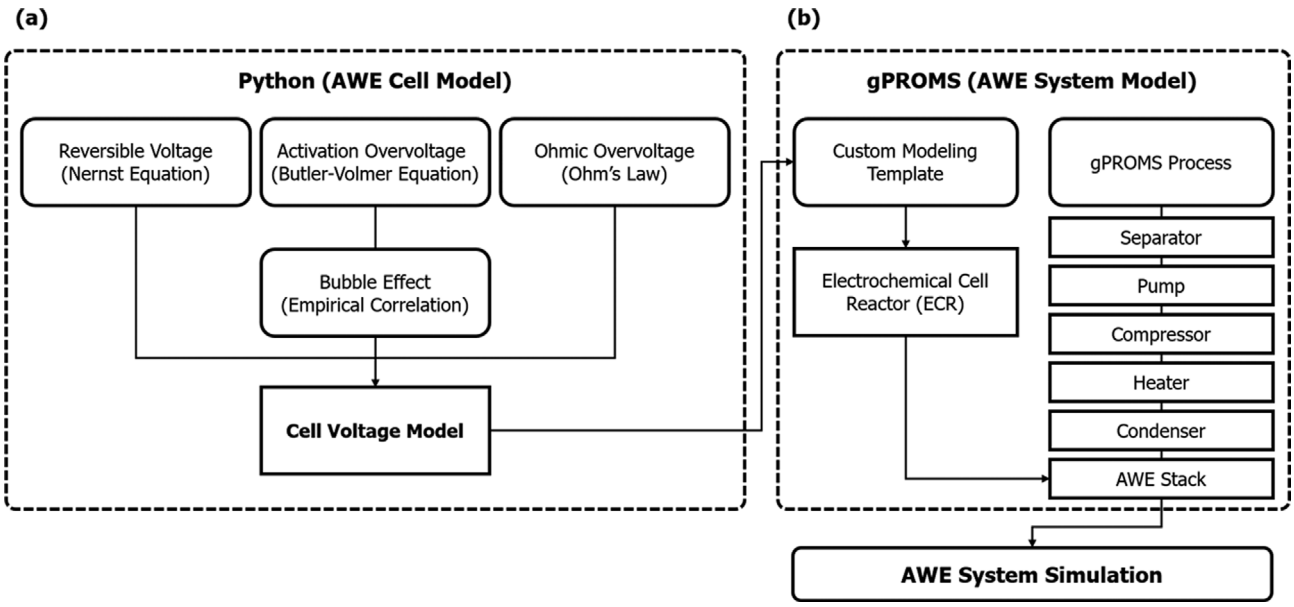

Fig. 2. Structure of AWE simulation model. (a) AWE cell in Python, and (b) AWE system in gPROMS.

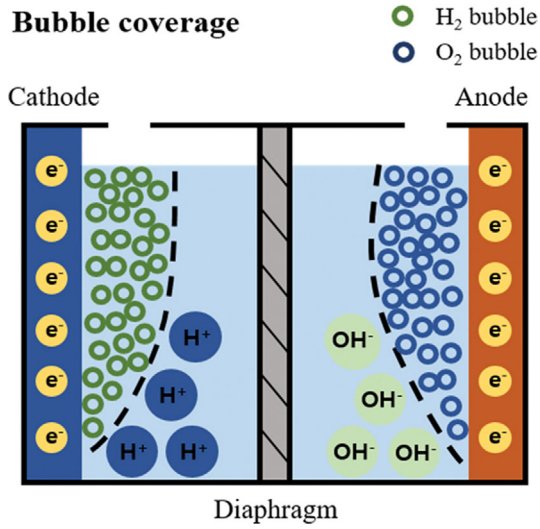

Fig. 3. Bubble coverage on the electrode surface.

$$P^{*}_{H_2O} = T^{-3.4159}\exp\left(37.043 - \frac{6275.7}{T}\right) \quad (8)$$

where T is the temperature (K), m is the molar concentration of the electrolyte, and w is the mass fraction of KOH.

Since an actual AWE cell requires electrical energy above the reversible voltage due to the internal resistance, the actual cell voltage (V_{cell}) is the sum of the reversible voltage (V_{rev}), the activation overvoltage (V_{act}), and the resistance overvoltage (V_{ohm}), it can be calculated as follows:

$$V_{cell} = V_{rev} + V_{act} + V_{ohm} \quad (9)$$

The activation overvoltage (V_{act}) represents the energy loss caused by the decrease in the electrochemical reaction rate at the electrolyte and the electrode surface. As shown in Fig. 3, it is caused by hydrogen and oxygen gas bubbles generated from the electrodes of the AWE cell. The activation overvoltage can be expressed by reflecting the decrease in the activation area due to the gas bubble effect in the Butler-Volmer equation, which shows the current-voltage relationship between the electrolyte and the electrode surface, and the Butler-Volmer equation is as follows:

$$V_{act} = \frac{RT}{\alpha_{an} zF}\ln\left(\frac{i}{i_{0,an}}\right) + \frac{RT}{\alpha_{ca} zF}\ln\left(\frac{i}{i_{0,ca}}\right) \quad (10)$$

where T, R, F, z are temperature (K), gas constant, Faraday constant, number of electrons exchanged per reaction, α_{an}, α_{ca} are charge transfer coefficients of anode and cathode, i is current density (A/cm^2), $i_{0,an}$, $i_{0,ca}$ are the exchange current density of the anode and cathode (A/cm^2). The charge transfer coefficient of the Ni electrode can be calculated by the formula obtained from experimental data, and can be calculated as follows [28]:

$$\alpha_{an} = 0.07835 + 0.001T \quad (11)$$

$$\alpha_{ca} = 0.1175 + 0.00095T \quad (12)$$

where T is the temperature (K). The exchange current density between the anode and the cathode can be calculated as follows using the data of the Ni electrode [28]:

$$i_{0,an} = 1.5\times10^{-4}\left(\frac{P}{P_{ref}}\right)^{0.1}\exp\left[-\frac{23000}{RT}\left(1-\frac{T}{T_{ref}}\right)\right] \quad (13)$$

$$i_{0,ca} = 0.9\times10^{-4}\left(\frac{P}{P_{ref}}\right)^{0.1}\exp\left[-\frac{42000}{RT}\left(1-\frac{T}{T_{ref}}\right)\right] \quad (14)$$

where T, P, R are the temperature (K), pressure (bar), and gas constants, and T_{ref}, P_{ref} are the reference temperature (K) and pressure (bar).

The effect of hydrogen and oxygen gas bubbles generated at the electrode can be expressed by an empirical correlation. When the current density increases, the amount of hydrogen and oxygen gas rises and the effect of the gas bubble increases, and the volume of the gas bubble changes according to temperature and pressure changes; consequently, the bubble coverage coefficient (θ) can be expressed by current density, temperature, and pressure as follows [24]:

$$\theta = 0.23(i)^{0.3}\left(\frac{T}{T_{ref}}\frac{P_{ref}}{P}\right)^{2/3} \quad (15)$$

where, T, P, i are temperature (K), pressure (bar), and current density (A/cm^2), and T_{ref}, P_{ref} are reference temperature (K) and pressure (bar). By reflecting the change in the electrode activation area by the bubble coverage coefficient to the electrode surface area of the Butler-Volmer equation, the activation overvoltage caused by hydrogen and oxygen gas bubbles can be calculated as follows:

$$V_{act} = \frac{RT}{\alpha_{an} zF}\ln\left(\frac{\frac{I}{S(1-\theta)}}{i_{0,an}}\right) + \frac{RT}{\alpha_{ca} zF}\ln\left(\frac{\frac{I}{S(1-\theta)}}{i_{0,ca}}\right) \quad (16)$$

$$= \frac{RT}{\alpha_{an} zF}\left\{\ln\left(\frac{i}{i_{0,an}}\right) - \ln(1-\theta)\right\} + \frac{RT}{\alpha_{ca} zF}\left\{\ln\left(\frac{i}{i_{0,ca}}\right) - \ln(1-\theta)\right\}$$

where S is the active area of the electrode (cm^2), I is the current (A), and θ is the bubble coverage coefficient.

The overvoltage (V_{ohm}) due to the resistance is generated in electrodes (R_{an}, R_{ca}), electrolyte (R_{ele}), and separator (R_{diaph}) as shown in Fig. 4, and overvoltage can be expressed by Ohm's law as follows:

$$V_{ohm} = I\times(R_{an} + R_{ca} + R_{ele} + R_{diaph}) \quad (17)$$

The resistance of the electrode, electrolyte, and separator was calculated based on the electrical conductivity of each material, and the resistance of the electrodes (R_{an}, R_{ca}) was calculated as follows [24]:

$$R_{an} = R_{ca} = \frac{1}{\sigma_{electrode}}\frac{L}{S} \quad (18)$$

where $\sigma_{electrode}$ is the electrical conductivity of the electrode (S/cm), and L, S are the thickness (cm) and active area of the electrode (cm^2). The resistance of the electrolyte (R_{ele}) was calculated based on the electrical conductivity of the KOH solution, and the increase in resistance due to the gas bubble inside the electrolyte was calculated as follows using the Bruggeman equation [29]:

$$\frac{R_{ele\text{-}bubble}}{R_{ele}} = (1-\varepsilon)^{-\frac{3}{2}} \quad (19)$$

$$\varepsilon = \frac{2}{3}\theta \quad (20)$$

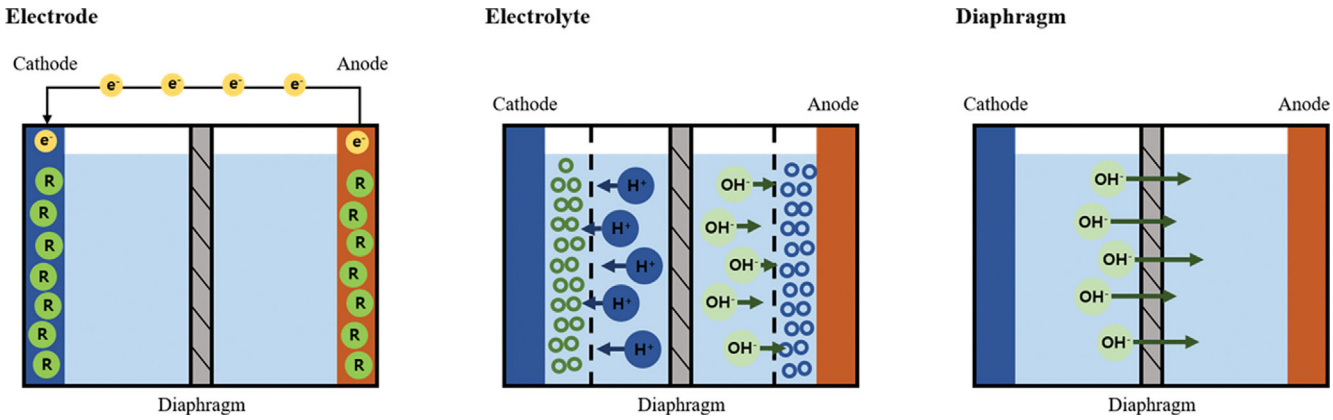

Fig. 4. Resistance at the electrode, electrolyte, and diaphragm.

$$R_{ele\text{-}bubble} = \frac{1}{\sigma_{electrolyte}(1-\varepsilon)^{3/2}}\left(\frac{d_{an\text{-}sep}}{S_{an}} + \frac{d_{ca\text{-}sep}}{S_{ca}}\right) \quad (21)$$

where $\sigma_{electrolyte}$ is the electrical conductivity of the electrolyte (S/cm), ε is the pore ratio, θ is the bubble coverage coefficient, S_{an}, S_{ca} are the active areas of the anode and cathode (cm^2), and $d_{an\text{-}sep}$, $d_{ca\text{-}sep}$ is the distance from the anode or cathode to the separator (cm). The resistance (R_{diaph}) of the separator was based on a 0.5 mm thick Zircon separator, and was calculated as follows [30]:

$$R_{diaph} = \frac{0.06 + 80e^{-T/50}}{10000 S_{diaph}} \quad (22)$$

where T is the temperature (K) and S_{diaph} is the cross-sectional area of the diaphragm (cm^2).

3. AWE System Model in gPROMS

The developed AWE cell model for cell voltage is integrated into the ECR library through the gPROMS custom modeling template to propose the AWE stack model. As a result, the liquid electrolyte effect was reflected by the mass fraction and vapor pressure of the KOH electrolyte, and the bubble effect of the gas generated inside the KOH liquid electrolyte by the electrochemical reaction can be explained through our AWE stack model in gPROMS.

With the AWE stack model, the AWE system simulation model was developed using the process equipment models such as separator, heater, condenser, pump, and compressor provided by gPROMS Process 2.1.1 [31]. Fig. 5 represents the process flow diagram of the AWE system depicted in gPROMS. The separator (Gas_Liquid_Separator) is a flash separator that separates the elec-

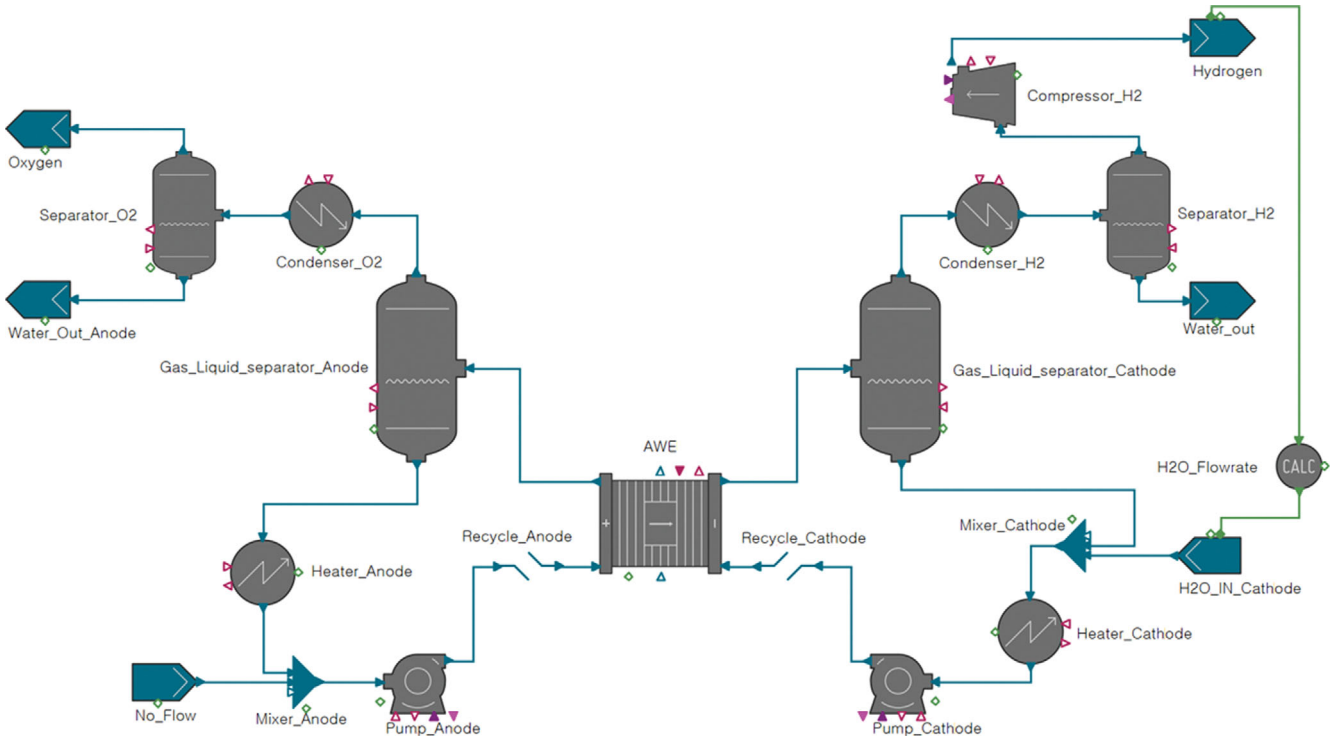

Fig. 5. AWE system simulation configuration in gPROMS.

trolyte mixed with hydrogen or oxygen gases from the AWE stack, and for the production of over 99% pure hydrogen, it undergoes an additional flash separation (Separator_H_2) after passing through the condenser. The condenser is set at 20 °C to condense the gas flow, removing electrolyte once again from the gas flow to increase the purity of the gas. The heater is responsible for raising the temperature of the electrolyte that has passed through the flash separator to the operating temperature of the AWE stack for recycling. The pump supplies the electrolyte back to the AWE stack, and both the mechanical efficiency and isentropic efficiency of the pump are set to 70%. The compressor, used for hydrogen compression, assumes polytropic compression, and both the mechanical efficiency and polytropic efficiency are assumed to be 70%, compressing the gas to a pressure of 200 bar. The total system energy consumption for energy efficiency analysis through the developed AWE system simulation is the sum of the energy consumption of the AWE stack and the energy consumption of the balance of plant (BOP) from gPROMS, and was calculated as follows:

$$W_{system}=W_{stack}+W_{heater_{an}}+W_{heater_{ca}}+W_{condenser_{O_2}}+W_{condenser_{H_2}}+W_{pump_{an}}+W_{pump_{ca}}+W_{compressor} \quad (23)$$

RESULTS AND DISCUSSION

1. Model Validation

The developed alkaline electrolysis cell model is a composite model constructed by integrating models from the literature, and it has been validated at various temperatures, current densities, and high pressures (1-100 bar) [22,24]. Additionally, the developed model was verified using the new experimental data of the AWE cell of the Korea Institute of Energy Research (KIER), which demonstrates the flexibility of the model used in this study. Table 1 shows the specifications of the AWE cell used in the experiment and modeling, the operating temperature range of the cell is 293.15-353.15 K, the operating pressure range is 1-7 bar, and a 30 wt% KOH solution is used as the electrolyte. The cell is rectangular, and it consists of an electrode, a porous transport layer (PTL), and a diaphragm; the electrode and diaphragm have a zero-gap structure. Electrodes are both Ni-based and these have the same structures: thickness is 0.7 mm, the porosity is 0.38%, and the active area of the electrode is 72,900 mm^2. The diaphragm is Zirfon UTP 500 with a thickness of 0.46 mm and an area of 72,900 mm^2. Fig. 6 is a diagram comparing the current-voltage polarization curves for the target AWE cell under the conditions of 80 °C and 1 bar. The AWE simulation model that integrated the Python-based cell model showed a value of 0.8 based on R-squared. The AWE simulation model showed a small error of 0.0296 V on average with the experimental data, but a relatively large error of up to 0.1449 V in the range of 0 to 0.1 A/cm^2. The maximum error appeared at a low current density of 0.01 A/cm^2. This error can be attributed to the dominance of the activation potential, which is significantly influenced by the bubble coverage, in cases of low current density. The bubble effect relies on empirical models derived from experiments conducted within the typical operating current density range of AWE cells. Therefore, the error is generally negligible due to the characteristics of an AWE system operating at a current density of 0.2 A/cm^2 or higher. In addition, for a current density of 0.2 A/cm^2 or more, it showed a high prediction accuracy of 0.985 based on R-squared and an error of 0.0079 V on average. The gPROMS model with the ECR library, which provides the physical and chemical properties of chemicals, complex mass transfer, and resistance inside the cell, displayed high accuracy.

Table 1. Alkaline water electrolysis cell and stack specification developed by KIER

Parameter	Unit	Value
Operating temperature	K	293.15-353.15
Operating pressure	bar	1-7
Electrolyte concentration	wt% KOH	30
Cell shape	-	Rectangular
Electrode-diaphragm distance	-	0 (Zero-gap)
Cathode material	-	$Ni_{0.9}Al_{0.1}$/Ni foam
Cathode thickness/porosity	mm/%	0.7/0.38
Cathode PTL thickness/porosity	mm/%	1.8/0.67
Cathode electrode area	mm^2	72,900
Anode material	-	$Ni_{0.5}Fe_{0.5}$/Fe foam
Anode thickness/porosity	mm/%	0.7/0.38
Anode PTL thickness/porosity	mm/%	1.8/0.67
Anode electrode area	mm^2	72,900
Diaphragm material	-	Zirfon UTP500
Diaphragm thickness/porosity	mm/%	0.46/0.53
Diaphragm active area	mm^2	72,900
Number of cells in stack	-	20
Stack size (L*H*W)	mm	171.2*530*470
End-plate area	mm	530*470
End-plate thickness	mm	25

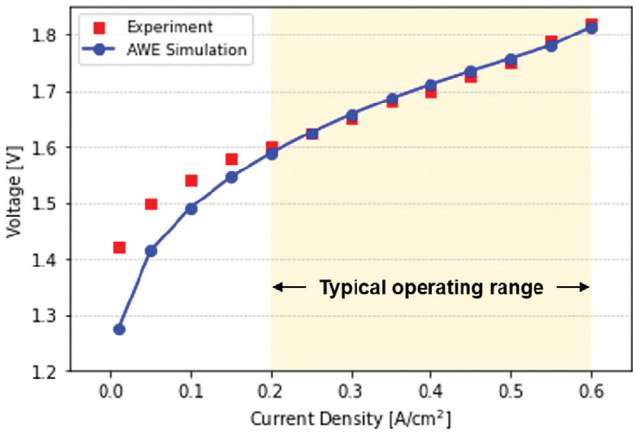

Fig. 6. Validation result of the simulation model.

2. AWE Cell Simulation Modules in Python

Fig. 7 is a flow diagram of a Python module for simulating an AWE cell according to operating temperature, pressure, and mass fraction of electrolyte based on existing literature. The cell voltage simulation module consists of four reversible voltage prediction models from three different literatures and five cell voltage prediction models (Cell Voltage Model in Fig. 7), from four different litera-

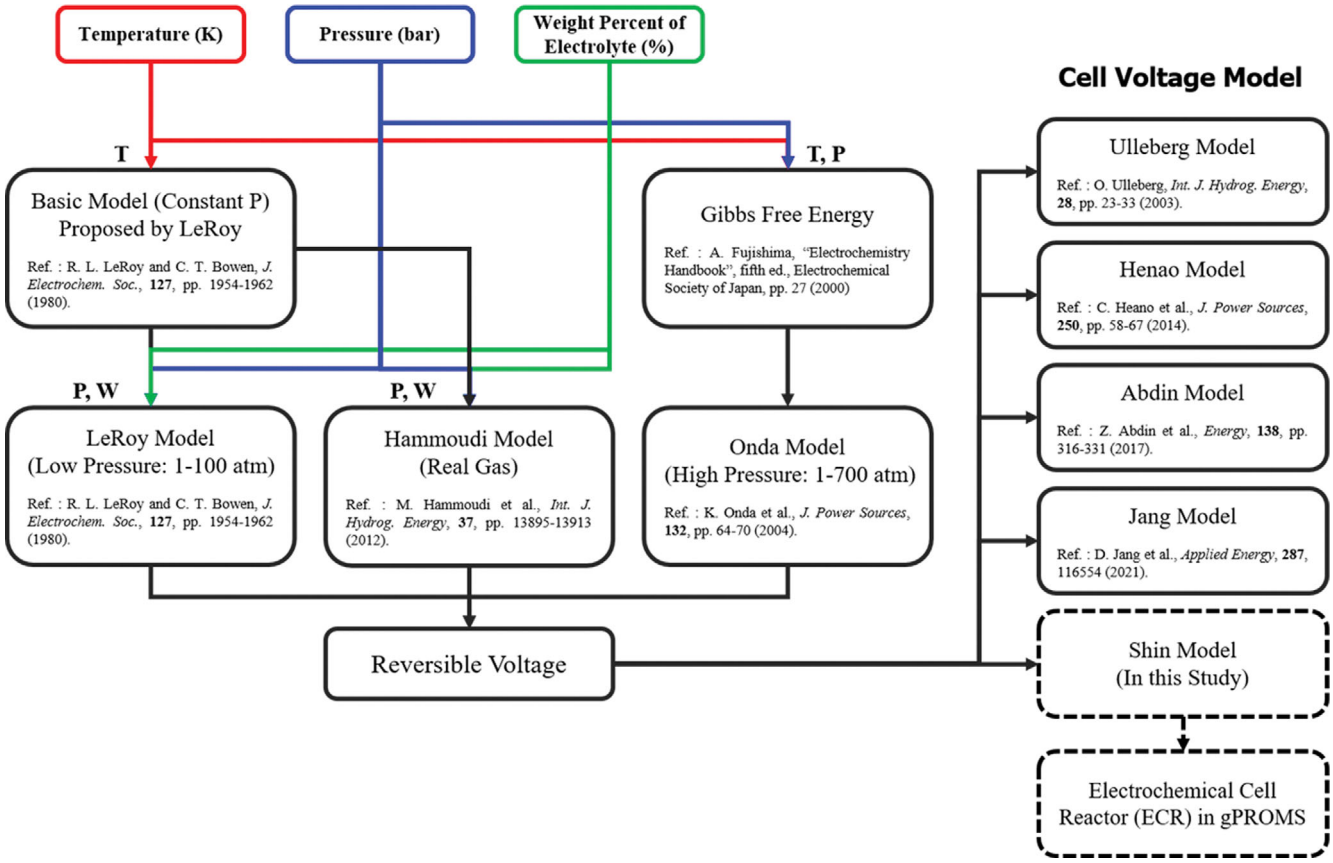

Fig. 7. Flow diagram of AWE cell simulation modules in Python.

Table 2. Python modules for AWE cell voltage simulation

Variable	Model	Features	Module
Reversible voltage	Constant pressure	Constant pressure (1 bar)	Reversible_Voltage().RV_ConstantP(T)
	LeRoy (1980)	Low pressure (1-100 bar)	Reversible_Voltage().RV_LeRoy(T, P, W)
	Onda (2004)	High pressure (1-700 bar)	Reversible_Voltage().RV_Onda(T, P)
	Hammoudi (2012)	Real gas	Reversible_Voltage().RV_Hammoudi(T, P, W)
Cell voltage	Ulleberg (2003)	Simple model	Cell_Voltage(T, P, W, I). CV_Ulleberg(A, r, t, s)
	Henao (2014)	Parameters: Structural properties	Cell_Voltage(T, P, W, I). CV_Henao(A, l, d)
	Abdin (2017)	Parameters: Material properties	Cell_Voltage(T, P, W, I). CV_Abdin(A, α, γ, i_0, G, ε, δ, d, β, τ, ω)
	Jang (2021)	High operating pressure	Cell_Voltage(T, P, W, I). CV_Jang(A, δ, d)

* T: Temperature [K], P: Pressure [bar], W: wt% of KOH [%], I: Current [A], i_0: Exchange current density [A/cm^2], A: Active area of electrode [m^2], l: Length of Electrode [cm], d: Length between electrode and separator [cm], δ: Thickness [cm], β: Width of bubble zone [cm], τ: Effective length [cm], ω: Wettability, r, t, s, α: Roughness factor

tures and the model developed in this study. The cell voltage simulation model developed in this study was integrated into the ECR library in gPROMS. Table 2 shows detailed parameters to simulate the AWE cell voltage for each model. Reversible voltage prediction models include a model according to temperature change at constant pressure (1 bar), low-pressure and high-pressure models, and a model that reflects the behavior of the actual gas according to the pressure increase. The cell voltage module has models which require the parameters for simulation based on: experimental data, structural characteristics, material characteristics, and system operation characteristics. This module can be quickly utilized for voltage prediction according to the operating conditions (temperature, high and low pressure, current density) of the AWE cell.

Fig. 8 shows the result of the simulation for the reversible voltage and cell voltage by the AWE cell Python module. Fig. 8(a) is the reversible voltage in the operating temperature range of 0-227 °C when the operating pressure is constant at 1 or 30 bar, Fig. 8(b) is reversible voltage simulation results using LeRoy, Onda, and Hammoudi models [15,22,27] in the operating pressure range of 1-700 bar when the temperature is constant at 25 °C and 80 °C. Revers-

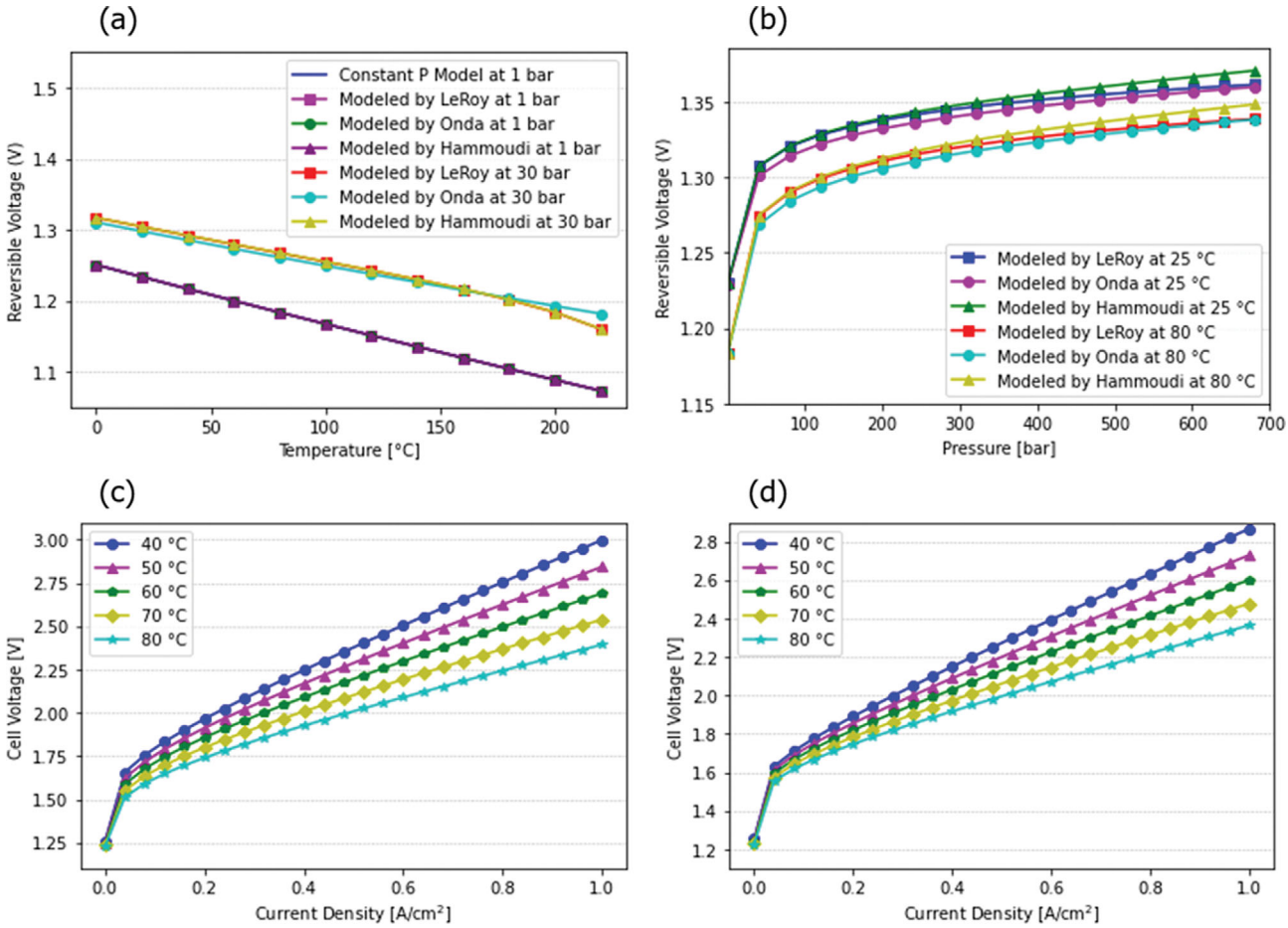

Fig. 8. AWE cell simulation results by Python modules. (a) reversible voltage with constant pressure, (b) reversible voltage with constant temperature, (c) cell voltage by Henao model, and (d) cell voltage by Abdin model.

ible voltage simulation is possible in various temperature and pressure ranges to suit the operation characteristics of AWE cells. Fig. 8(c) and (d) are the cell voltage simulation results under the temperature condition of 40-80 °C for the current density range of 0-1.0 A/cm^2 using the Hanao and Abdin model [16,17]. AWE cell characteristic parameters for each simulation were obtained by referring to the data of each literature. The Python-based AWE cell simulation module provides reversible voltage and cell voltage simulation over a wide range of temperature, pressure, and current density.

3. Simulation Results in gPROMS

AWE system simulation was performed by integrating the model developed in this study among the cell voltage models constituting the Python-based module into gPROMS. Assuming a scenario in which hydrogen produced from the AWE system is compressed to 200 bar for loading on a tube trailer, the simulation of the entire green hydrogen production process was performed using gPROMS. AWE system simulation scenarios using gPROMS are as shown in Table 3, three current densities (0.2, 0.4, 0.6 A/cm^2), three temperatures (40, 60, 80 °C), and six pressures (1, 5, 10, 30, 60, 100 bar), simulation for the energy consumption of whole process including the compression and BOP was performed for a total of 54 cases.

In 54 cases, the energy efficiency of the AWE system was evaluated, and the optimal operating conditions of the system were analyzed. The energy efficiency is calculated as follows:

Table 3. AWE simulation scenarios in gPROMS

Current density [A/cm^2]	Temperature [°C]	Pressure [bar]	Number of cases
0.2	40		6
	60	1, 5, 10, 30, 60, 100	6
	80		6
0.4	40		6
	60	1, 5, 10, 30, 60, 100	6
	80		6
0.6	40		6
	60	1, 5, 10, 30, 60, 100	6
	80		6

$$\text{Energy efficiency} = \frac{\text{Rate of hydrogen production (mol/h)}}{\text{Energy consumption of whole process (kW)}} \quad (24)$$

Fig. 9 shows the energy consumption (left) of the entire system according to operating temperature, pressure, and current density, excluding the energy consumed for compression of hydrogen produced from the AWE system, and the energy efficiency (right),

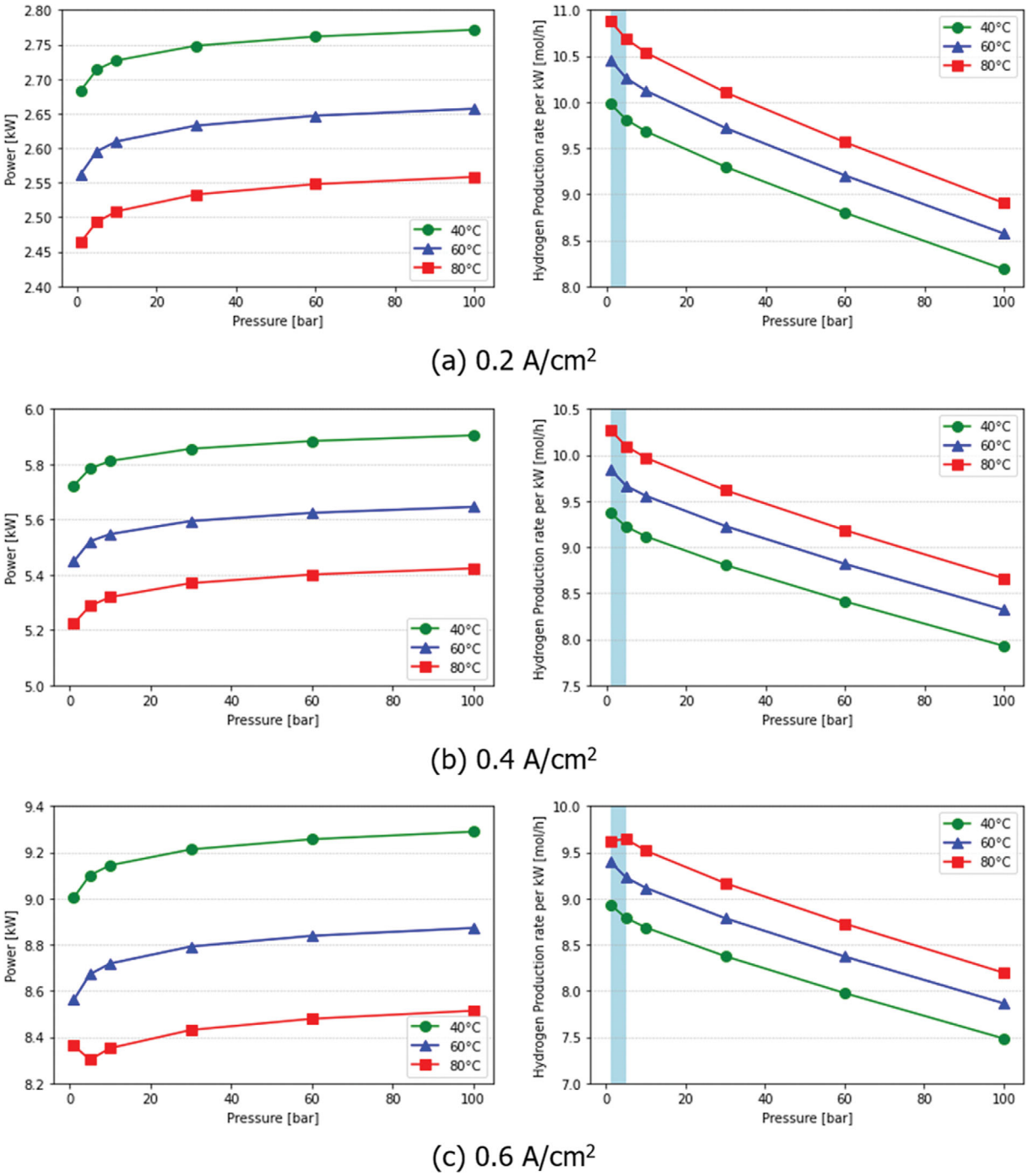

Fig. 9. Total power consumption and hydrogen production efficiency without compression power.

hydrogen production rate divided by the total energy consumption. For current densities of 0.2 and 0.4 A/cm^2, the energy consumption of the system increases as the pressure increases, and the energy efficiency is higher at the lower pressure. On the other hand, when the current density was 0.6 A/cm^2, the highest efficiency was exhibited at a pressure of 5 bar. Because the reversible voltage, which is the theoretically required energy of the AWE stack, increases as the pressure increases under the corresponding conditions (Eq. (5)), and the volume of the generated gas bubble decreases (Eq. (15)). This phenomenon causes that the overvoltage (V_{act}) reduction effect by the gas bubble is superior to the reversible potential (V_{rev}) rise. Therefore, the energy efficiency is temporarily increased at a pressure of 5 bar.

Fig. 10 is a diagram showing the energy consumption (left) and energy efficiency (right) of the entire system according to operating temperature, pressure, and current density, including the energy consumption of the compressor that compresses the produced hydrogen to 200 bar. When the compression is included in the

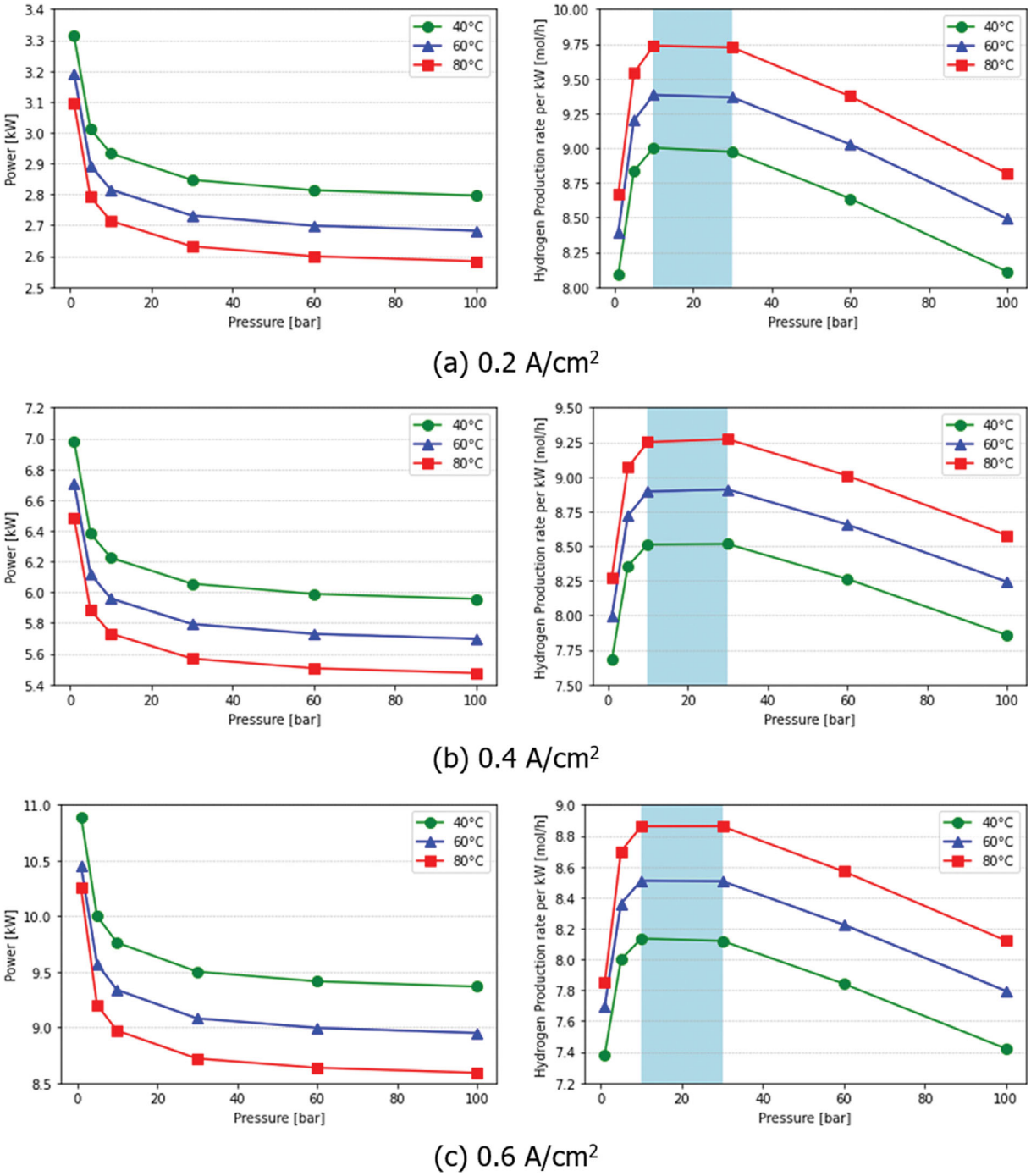

Fig. 10. Total power consumption and hydrogen production efficiency with compression power.

AWE system, the energy consumption of the entire system is lower at the higher operating pressure. However, when the operating pressure increases, the hydrogen production rate decreases uniformly as shown in Fig. 11 because of the reduction of Faraday efficiency. The decrease rate of the total energy consumption (energy saving) becomes smaller with rising the pressure, and finally the decrease rate of hydrogen production and energy saving rate intersect at 30 bar, which means the loss of the hydrogen production is higher than the benefit obtained by saving compression energy after 30 bar. Therefore, hydrogen production efficiency declines above 30 bar. The hydrogen production efficiency is the highest at 10-30 bar; therefore, it is advantageous to operate the AWE system at 10-30 bar when compression for storage and transportation of hydrogen is considered. When assuming compression up to 700 bar, it is observed that the energy consumption of the compressor increases at low pressures, resulting in a point where the total energy consumption decrease and the hydrogen production rate decrease intersect at a higher pressure compared to the 200 bar case. Therefore,

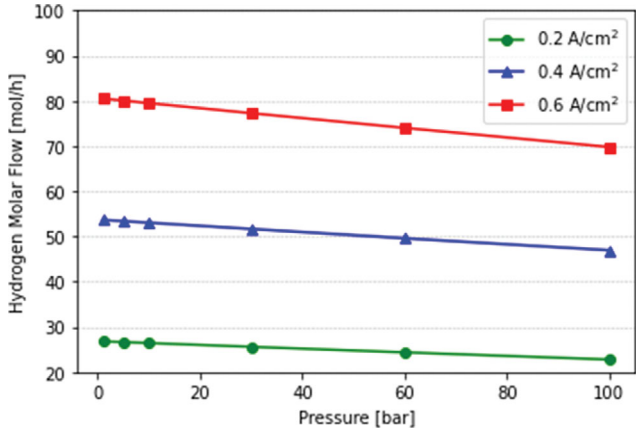

Fig. 11. Hydrogen production rate according to the pressure at 80 °C and 0.2, 0.4, 0.6 A/cm^2.

considering hydrogen compression, pressures above 10 bar are always advantageous.

Table 4 shows the energy consumption, hydrogen production, and hydrogen production efficiency of the entire system, such as the AWE stack and BOP, when the current density is 0.2 A/cm^2. As the temperature increases, the power consumption of the BOP increases, but the overall energy consumption decreases because the effect of the decrease of the AWE stack power is dominant. When the operating temperature is 80 °C and the pressure is 100 bar, the energy consumption is the smallest at 2.584 kW, but the energy efficiency shows the highest efficiency at 9.737 mol/h·kW at 80 °C and 10 bar.

Table 5 shows the energy consumption, hydrogen production, and hydrogen production efficiency of the entire system when the current density is 0.4 A/cm^2. Although the current density increased, the effect of the temperature increase was constant, and the energy consumption was 5.475 kW under the operating conditions of 80 °C and 100 bar. However, it showed the highest energy efficiency of 9.272 mol/h·kW at 80 °C and 30 bar. As the current density increases, the hydrogen production increases proportionally, which increases the effect of reducing the water electrolysis efficiency due to the bubble effect (Eq. (15) and (16)). When the pressure increases at a high current density, the effect of canceling the bubble effect increases. Therefore, the decrease in hydrogen production becomes smaller, showing the optimum hydrogen production efficiency at high pressure compared to low current density.

Table 6 illustrates the energy consumption, hydrogen production, and hydrogen production efficiency of the entire system at the current density of 0.6 A/cm^2. The same phenomenon as in the case of the current density of 0.4 A/cm^2 is shown, and energy consumption is 8.591 kW under the operating conditions of 80 °C and 100 bar. It indicates the highest energy efficiency of 8.861 mol/h·kW at 80 °C and 30 bar. When the operating temperature is high, hydrogen production efficiency is superior, but in the case of an AWE system linked to renewable energy with load fluctuations, frequent start/stop is required; it would be disadvantageous because of the long start-up time. When the current density increases, the absolute hydrogen production increases, but the hydrogen production efficiency decreases.

Table 4. Power consumption and hydrogen production efficiency at 0.2 A/cm^2

Pressure [bar]	Stack power [kW]	Total BOP [kW]	Comp. power [kW]	Power w/o comp. [kW]	Total power [kW]	H_2 rate [mol/h]	H_2 rate per kW w/o comp.	H_2 rate per kW
Temperature: 40 °C								
1	2.547	0.137	0.630	2.683	3.313	26.788	9.983	8.086
5	2.577	0.136	0.299	2.714	3.013	26.614	9.808	8.834
10	2.591	0.136	0.206	2.727	2.932	26.399	9.681	9.002
30	2.612	0.136	0.099	2.748	2.847	25.547	9.296	8.973
60	2.626	0.136	0.052	2.762	2.813	24.298	8.799	8.637
100	2.636	0.135	0.025	2.771	2.796	22.680	8.184	8.110
Temperature: 60 °C								
1	2.415	0.148	0.630	2.562	3.192	26.796	10.458	8.395
5	2.450	0.145	0.299	2.595	2.894	26.626	10.260	9.199
10	2.465	0.144	0.206	2.610	2.815	26.415	10.122	9.383
30	2.489	0.144	0.099	2.633	2.732	25.583	9.718	9.366
60	2.503	0.143	0.052	2.647	2.699	24.360	9.204	9.027
100	2.514	0.143	0.025	2.657	2.682	22.776	8.572	8.491
Temperature: 80 °C								
1	2.293	0.171	0.630	2.464	3.094	26.808	10.881	8.665
5	2.338	0.155	0.299	2.493	2.792	26.639	10.685	9.539
10	2.355	0.154	0.206	2.508	2.714	26.427	10.536	9.737
30	2.380	0.152	0.099	2.533	2.632	25.593	10.105	9.724
60	2.396	0.151	0.052	2.548	2.600	24.367	9.564	9.373
100	2.408	0.150	0.025	2.558	2.584	22.779	8.904	8.817

Table 5. Power consumption and hydrogen production efficiency at 0.4 A/cm^2

Pressure [bar]	Stack power [kW]	Total BOP [kW]	Comp. power [kW]	Power w/o comp. [kW]	Total power [kW]	H_2 rate [mol/h]	H_2 rate per kW w/o comp.	H_2 rate per kW
Temperature: 40 °C								
1	5.492	0.230	1.260	5.722	6.982	53.622	9.371	7.680
5	5.555	0.229	0.599	5.784	6.384	53.335	9.221	8.355
10	5.583	0.229	0.413	5.812	6.224	52.977	9.115	8.511
30	5.627	0.229	0.199	5.856	6.055	51.563	8.805	8.515
60	5.656	0.228	0.105	5.884	5.989	49.488	8.411	8.263
100	5.677	0.228	0.052	5.905	5.956	46.802	7.927	7.857
Temperature: 60 °C								
1	5.196	0.252	1.261	5.448	6.708	53.635	9.845	7.995
5	5.271	0.250	0.600	5.521	6.120	53.353	9.664	8.717
10	5.301	0.246	0.413	5.547	5.960	53.004	9.556	8.894
30	5.350	0.245	0.200	5.594	5.794	51.621	9.227	8.909
60	5.380	0.244	0.105	5.624	5.729	49.591	8.818	8.655
100	5.403	0.243	0.052	5.646	5.698	46.961	8.318	8.242
Temperature: 80 °C								
1	4.924	0.299	1.261	5.223	6.484	53.655	10.273	8.275
5	5.020	0.267	0.600	5.287	5.887	53.373	10.095	9.067
10	5.055	0.264	0.413	5.319	5.732	53.023	9.969	9.251
30	5.108	0.262	0.200	5.369	5.569	51.637	9.617	9.272
60	5.141	0.260	0.105	5.401	5.506	49.602	9.184	9.008
100	5.165	0.258	0.052	5.423	5.475	46.964	8.660	8.578

Table 6. Power consumption and hydrogen production efficiency at 0.6 A/cm^2

Pressure [bar]	Stack power [kW]	Total BOP [kW]	Comp. power [kW]	Power w/o comp. [kW]	Total power [kW]	H_2 rate [mol/h]	H_2 rate per kW w/o comp.	H_2 rate per kW
Temperature: 40 °C								
1	8.637	0.367	1.891	9.004	10.894	80.444	8.934	7.384
5	8.736	0.365	0.899	9.101	10.000	79.984	8.789	7.999
10	8.779	0.365	0.618	9.144	9.762	79.411	8.685	8.135
30	8.848	0.364	0.288	9.212	9.501	77.145	8.374	8.120
60	8.893	0.364	0.157	9.257	9.414	73.821	7.975	7.842
100	8.926	0.363	0.077	9.289	9.367	69.518	7.484	7.422
Temperature: 60 °C								
1	8.161	0.400	1.891	8.561	10.452	80.463	9.399	7.699
5	8.280	0.391	0.899	8.671	9.571	80.012	9.227	8.360
10	8.328	0.390	0.619	8.718	9.337	79.452	9.114	8.510
30	8.403	0.389	0.289	8.792	9.081	77.237	8.785	8.506
60	8.451	0.387	0.157	8.838	8.996	73.985	8.371	8.225
100	8.487	0.386	0.077	8.872	8.950	69.771	7.864	7.796
Temperature: 80 °C								
1	7.893	0.470	1.892	8.364	10.255	80.493	9.624	7.849
5	7.879	0.422	0.900	8.301	9.201	80.043	9.643	8.700
10	7.934	0.418	0.619	8.352	8.971	79.482	9.517	8.860
30	8.016	0.414	0.289	8.430	8.719	77.262	9.165	8.861
60	8.067	0.412	0.157	8.479	8.636	74.001	8.728	8.569
100	8.105	0.408	0.077	8.514	8.591	69.775	8.196	8.122

When the hydrogen compression process is not considered, it is advantageous to operate at a low pressure of 1-10 bar [23,24], but considering the hydrogen compression process, operating at a pressure of 10-30 bar is advantageous in terms of hydrogen production efficiency. However, in high-pressure operation, there may be material restrictions that make up the AWE stack; moreover, when an AWE system is operated at 1 MPa (=10 bar) or higher, it is subject to legal regulations according to Article 2, Paragraph 1 of the High-Pressure Gas Safety Control Act in Korea. Therefore, it is necessary to consider compression for storage, transportation, and utilization to expand the supply of green hydrogen, rather than analyzing the efficiency of a simple system, and additionally consider material constraints according to operating conditions, ease of maintenance, and social regulations.

CONCLUSIONS

Hydrogen produced through the water electrolysis system requires high-pressure compression for transportation, storage, and charging. An AWE system simulation model was proposed to evaluate the effects of the compression to the energy consumption and efficiency in the whole process. In this study, a Python module was designed by AWE cell voltage models which include models from several literatures and the model developed in this study. The Python module can be applied to voltage prediction according to the operating conditions of the AWE cell. With the cell voltage model developed in this study, the AWE system simulation model was proposed by integrating the developed model into gPROMS including the compression process.

Considering the energy required to compress the hydrogen to 200 bar, the energy consumption and hydrogen production efficiency according to the operating pressure, temperature, and current density of the AWE system were analyzed by the simulation model. When the hydrogen compression process was not considered, the optimum operating pressure was 1-10 bar, but when the energy consumed for hydrogen compression was considered, the energy efficiency was the highest at 10-30 bar. The actual system for green hydrogen production has superior energy efficiency at the pressure of 10 bar or more in consideration of the hydrogen compression process. Nevertheless, in the case of the high-pressure operation, material restrictions may occur that constitute the AWE system. In Korea, it is regulated by the High-Pressure Gas Safety Control Act operated at 1 MPa (=10 bar) or higher. Therefore, to optimize the operation of the actual water electrolysis system including the compression process, material constraints and social regulations should be considered.

ACKNOWLEDGEMENTS

This research was partly supported by Korea Institute of Energy Technology Evaluation and Planning (KETEP) grant funded by the Korea government (MOTIE) (20207200000070, Development of performance standardization and operation risk estimation for renewable energy-linked alkaline water electrolysis hydrogen production systems using digital twins) and Korea Institute for Advancement of Technology (KIAT) grant funded by the Korea Government (MOTIE) (P0008475, Development Program for Smart Digital Engineering Specialist).

DECLARATION OF COMPETING INTEREST

The authors declare that they have no known competing financial interests or personal relationships that could have appeared to influence the work reported in this paper.

REFERENCES

1. IPCC, Global Warming of 1.5 °C. An IPCC Special Report (2018).
2. X. Shao, Y. Zhong, Y. Li and M. Altuntaş, *J. Environ. Manage.*, **296**, 113229 (2021).
3. E. Agora, The European Power Sector in 2020: Up-to-Date Analysis on the Electricity Transition (2021).
4. U.S. Energy Information Administration, Monthly Energy Review, November (2021).
5. A. Olabi, *Energy*, **136**, 1 (2017).
6. National Renewable Energy Laboratory, Declining Renewable Costs Drive Focus on Energy Storage (2020).
7. N. Khan, S. Dilshad, R. Khalid, A. R. Kalair and N. Abas, *Energy Storage*, **1**(3), e49 (2019).
8. S. B. Walker, U. Mukherjee, M. Fowler and A. Elkamel, *Int. J. Hydrog. Energy*, **41**(19), 7717 (2016).
9. IRENA, Green Hydrogen Cost Reduction: Scaling up Electrolysers to Meet the 1.5 °C Climate Goal, International Renewable Energy Agency, Abu Dhabi (2020).
10. M. Götz, J. Lefebvre, F. Mörs, A. M. Koch, F. Graf, S. Bajohr, R. Reimert and T. Kolb, *Renew. Energy*, **85**, 1371 (2016).
11. M. David, C. Ocampo-Martínez and R. Sánchez-Peña, *J. Energy Storage*, **23**, 392 (2019).
12. Z. Dobó and Á. B. Palotás, *Int. J. Hydrog. Energy*, **42**(9), 5649 (2017).
13. M. Suermann, T. J. Schmidt and F. N. Büchi, *Electrochim. Acta*, **211**, 989 (2016).
14. O. Ulleberg, *Int. J. Hydrog. Energy*, **28**(1), 21 (2003).
15. M. Hammoudi, C. Henao, K. Agbossou, Y. Dub and M. Doumbia, *Int. J. Hydrog. Energy*, **37**(19), 13895 (2012).
16. C. Henao, K. Agbossou, M. Hammoudi, Y. Dub and A. Cardenas, *J. Power Sources*, **250**, 58 (2014).
17. Z. Abdin, C. Webb and E. Gray, *Energy*, **138**, 316 (2017).
18. H. Kojima, T. Matsuda, H. Matsumoto and T. Tsujimura, *J. Int. Counc. Electr. Eng.*, **8**(1), 19 (2018).
19. M. Sánchez, E. Amores, D. Abad, L. Rodríguez and C. Clemente-Jul, *Int. J. Hydrog. Energy*, **45**(7), 3916 (2020).
20. D. Jang, W. Choi, H. Cho, W. C. Cho, C. H. Kim and S. Kang, *J. Power Sources*, **506**, 230106 (2021).
21. C. Azzaro-Pantel, Cambridge, Massachusetts, US: Academic Press (2018).
22. K. Onda, T. Kyakuno, K. Hattori and K. Ito, *J. Power Sources*, **132**(1-2), 64 (2004).
23. A. Roy, S. Watson and D. Infield, *Int. J. Hydrog. Energy*, **31**(14), 1964 (2006).
24. D. Jang, H. Cho and S. Kang, *Appl. Energy*, **287**, 116554 (2021).
25. M. Minutillo, A. Perna, A. Forcina, S. D. Micco and E. Jannelli, *Int. J. Hydrog. Energy*, **46**(26), 13667 (2021).

26. B. Bensmann, R. Hanke-Rauschenbach, G. Müller-Syring, M. Henel and K. Sundmacher, *Appl. Energy*, **167**, 107 (2016).
27. R. L. Leroy, C. T. Bowen and D. J. Leroy, *J. Electrochem. Soc.*, **127**(9), 1954 (1980).
28. D. Henao and C. Christian, Trois-Rivières, Universit du Québec Trois-Rivières (2011).
29. M. P. M. G. Weijs, L. J. J. Janssen and G. J. Visser, *J. Appl. Electrochem.*, **27**, 371 (1997).
30. P. Vermeiren, *Int. J. Hydrog. Energy*, **23**(5), 321 (1998).
31. Y. Shin, J. Oh, D. Jang and D. Shin, *Comput. Aided Chem. Eng.*, **49**, 1483 (2022).